Journal of Power Sources 196 (2011) 6449–6455

Contents lists available at ScienceDirect

Journal of Power Sources

journal homepage: www.elsevier.com/locate/jpowsour

Strategic dispersion of carbon black and its application to ink-jet-printed lithium cobalt oxide electrodes for lithium ion batteries

Jin-Hyon Lee [a], Sung-Bok Wee [a], Moon-Seok Kwon [b], Hyun-Ho Kim [a], Jae-Man Choi [b], Min Sang Song [b], Ho Bum Park [c], Hansu Kim [c,*], Ungyu Paik [a,c,**]

[a] Division of Materials Science Engineering, Hanyang University, Seoul 133-791, Republic of Korea
[b] Energy Lab., Samsung Advanced Institute of Technology, Samsung Electronics Co. Ltd., Suwon 440-600, Republic of Korea
[c] WCU Department of Energy Engineering, Hanyang University, Seoul 133-791, Republic of Korea

ARTICLE INFO

Article history:
Received 23 December 2010
Received in revised form 8 March 2011
Accepted 9 March 2011
Available online 31 March 2011

Keywords:
Surface modification
Carbon black
Dispersion properties
Ink
Lithium ion battery

ABSTRACT

The effects of surface-modified carbon black induced by UV/ozone and triethylenetetramine on the microstructure and electrochemical properties of ink-jet-printed $LiCoO_2$ electrodes for lithium ion batteries are observed. The dispersion properties of surface-modified carbon black and $LiCoO_2$ ink are evaluated using particle size distribution measurements, surface pressure calculations, and scanning electron microscopy. Modifications to the surface of carbon black result in improved dispersion properties, which in turn enhance the compactness and homogeneity of the microstructure of ink-jet-printed $LiCoO_2$ electrodes compared to those printed with as-received carbon black. Electrochemical experiments indicate that $LiCoO_2$ electrodes ink-jet-printed with surface-modified carbon black exhibit improved initial specific discharge capacities compared to those printed with as-received carbon black due to the better electrical contact between the carbon black and the $LiCoO_2$, as evidenced by the analysis of the area-specific impedance of the electrode as a function of the depth of discharge.

1. Introduction

State-of-the-art electronic technologies require flexible thin-film batteries as the power sources for portable electronic devices such as flexible displays, smart cards, active radio-frequency identification tags, electronic paper, and wearable devices [1]. Various fabrication processes for thin film batteries have been explored, including RF magnetron sputtering [2–4] and electron beam evaporation [5,6]. However, these methods have several disadvantages, for example, the high production cost caused by the use of complicated and costly equipment and low throughput, which must be addressed for the purposes of commercialization [7].

Ink-jet printing is an attractive way to prepare thin films due to low production costs, ease of mass production, and a broad choice of substrates [7]. Several studies on the electrochemical properties of electrodes prepared using the ink-jet printing method have been reported [7–10]. Huang et al. [8] prepared $LiCoO_2$ thin film electrodes with a thickness of about 1.2 μm using an ink-jet printing method that showed an initial discharge capacity of 120 mAh g^{-1} and a capacity retention of 95% after 100 cycles. However, they observed a gradual increase in the charge transfer resistance after 50 cycles due to electrical contact loss between the solid phases [8], implying that dispersion of the solid phases in the ink was problematic. The electrical contact between the solid phases is determined by the microstructures of the composite electrodes, which might depend on the dispersion stability of the solid phases [11]. To improve the electrical contact between the solid phases, carbon black, acting as a conducting agent, must be homogeneously distributed around each active particle and provide conducting paths between them [12,13]. Therefore, it is crucial to homogeneously disperse both the active materials and the carbon black within the ink to improve the electrical contact between the solid phases. Recently, Patey et al. reported a method that is effective for achieving better dispersions of the anatase TiO_2 and carbon black in n-methyl-2-pyrrolidone (NMP) using a turbo-stirrer [12]. However, due to the relatively high Hamaker constant of carbon black ($\sim 6.7 \times 10^{-20}$ J) [14] and the poor compatibility between hydrophobic carbon black and NMP (polar energy ~ 12.3 $MPa^{1/2}$ [15]), a physical mixing technique might not completely guarantee homogeneous dispersion of the carbon black. Therefore, modifying the carbon black surface from a state of hydrophobicity to one of hydrophilicity would increase the compatibility between the carbon black and the NMP, improving the dispersion properties of the carbon black in the liquid medium.

* Corresponding author. Tel.: +82 2 2220 2412; fax: +82 2 2281 0502.
** Corresponding author at: WCU Department of Energy Engineering, Hanyang University, 17 Haengdang-dong, Seongdong-gu, Seoul 133-791, Republic of Korea. Tel.: +82 2 2220 0502; fax: +82 2 2281 0502.
E-mail addresses: khansu@hanyang.ac.kr (H. Kim), upaik@hanyang.ac.kr (U. Paik).

0378-7753/$ – see front matter © 2011 Elsevier B.V. All rights reserved.
doi:10.1016/j.jpowsour.2011.03.041

Various approaches based on chemical oxidation processes have been suggested to modify the surfaces of the carbon nanoparticles using highly concentrated acids such as HNO_3, H_2SO_4 or their mixtures, and $KMnO_4$ [16,17]. However, these methods result in the formation of defects in the carbon. For example, the acid treatment results in the introduction of structural defects along the wall at the caps of the carbon nanotubes, which severely degrades their electrical properties [18]. Ultra-violet/ozone (UV/ozone) and triethylenetetramine (TETA) treatments to functionalize the surfaces of the nanotubes [19] were reported to be milder approaches than chemical oxidation. UV/ozone and TETA treatments provide the surfaces of the nanotubes with carboxylic and amine functional groups, respectively, producing a surface change from a hydrophobic to a hydrophilic state. Indeed, surface modifications of carbon nanotubes using UV/ozone and TETA treatments were reported to lead to improved dispersion of carbon nanotubes in epoxy resin [19].

In this work, sequential treatments of UV/ozone and TETA were exploited as a method to improve the dispersion properties of carbon black in NMP by improving the compatibility between them. The effects of surface-modified carbon black (CB) on the microstructural changes and electrochemical properties of ink-jet-printed $LiCoO_2$ electrodes were studied. The surface of the CB was modified using UV/ozone and TETA treatments. The surface modification effects on the dispersion properties of CB and $LiCoO_2$ ink were characterized through particle size distribution analysis, surface pressure evaluations, scanning electron microscopy, and pore size measurements. The influence of the surface-modified CB on the electrochemical properties of ink-jet-printed $LiCoO_2$ electrodes was examined using a coin-type half cell. Hydrophilic functional groups were formed on the CB surfaces, which resulted in improved dispersion properties in NMP, and the electrode ink-jet printed with surface-modified CB showed improved electrochemical properties compared to those of an electrode printed with the as-received CB, which might be due to better electrical contact between the solid phases in the composite electrodes.

2. Experiment

2.1. Synthesis of nanosized $LiCoO_2$

Nanosized $LiCoO_2$ was synthesized using a modified Pechini method [20,21]. A stoichiometric amount of Li_2CO_3 (Aldrich) was dissolved in deionized water. Then, $Co(CH_3COO)_2{\cdot}4H_2O$ (Aldrich) was added to the Li_2CO_3 solution. Citric acid (Aldrich) and ethylene glycol solution (Aldrich) in HNO_3 (Aldrich) were then added. The solution was heated and stirred to obtain a viscous resin, which was charred to ash upon further heating. The ash was then calcined at 700 °C for 10 h to complete the reaction. The process used in this work is detailed elsewhere [20,21]. The morphology and size for as-synthesized $LiCoO_2$ nanoparticles were observed using scanning electron microscopy (SEM, S-4500, Hitachi, Japan).

2.2. Surface treatment of carbon black

Carbon black (Super P, average particle size ≈ 40 nm) was dried at 80 °C overnight, and then 0.5 g of the dried powder was placed in a UV-ozone generator (Ozonecure 16, Minuta Technology Co. Ltd., Korea) in ambient atmosphere at varying durations of up to 2 h. During the UV/ozone treatment, the CB was shaken at 10 min intervals for a uniform exposure. The UV output at a distance of 20 mm from the lamp was 120 μW cm^{-2} at a wavelength of 254 nm. Atomic oxygen was generated when the ambient oxygen was dissociated by irradiation at 184.9 nm and ozone at 253.7 nm. The UV/ozone-treated carbon black was further modified with an additional treatment of triethylenetetramine (TETA, Aldrich). The CB was mixed with TETA solution and sonicated at 60 °C for 1 h. The mixture was rinsed using excess acetone and filtrated.

2.3. $LiCoO_2$ ink and electrode preparation

The synthesized $LiCoO_2$ (232.5 mg) and CB (7.5 mg) were homogeneously mixed using an agate mortar and pestle, and then 0.2 g of 5 wt% of PVDF (6020, Solvay Solexis, Belgium, MW = 687,000) stock solution and additional solvent (4.56 g) were added to the mixture. NMP (Aldrich) was used as a solvent. The mass fraction of the solid phase was 5 wt%. Then, the ink was sonicated for 5 h, transferred into a cartridge and printed using an ink-jet printer (Fujifilm Dimatix Inc., Santa Clara, CA, USA). Aluminum foil was used as an electrode substrate. The thickness of the printed $LiCoO_2$ electrode was adjusted by controlling the number of printing repetitions. The electrode thickness was about 20 μm before pressing. The printed electrode was dried at about 120 °C in a vacuum oven for 2 h. The printed $LiCoO_2$ electrode consists of a mixture of 93 wt% of active material, 3 wt% CB and 4 wt% PVDF binder based on the total solid contents.

2.4. Characterization

Diffuse reflectance Fourier transform infrared spectroscopy (DRIFTS) samples were prepared by mixing the dried powders with KBr at a weight ratio of 5/95 using an agate mortar and pestle. The samples were studied using a spectrometer (Model Magna IR 550, Nicolet Instruments Corp., Madison, WI) equipped with a triglycerine sulfate (TGS) detector and were mounted with a diffuse reflectance cell (Model Collector™, Spectra-Tech, Inc., Shelton, CT) in the optics chamber. The chamber was purged with filtered N_2 (g), which eliminated the H_2O (g) and CO_2 (g) from the inlet stream. Each spectrum was acquired at a resolution of 4 cm^{-1} and represents an average of 128 scans. The particle size distribution (APS, Matec Applied Science, Hopkinton, MA, USA) was measured to investigate the effect of surface modification of CB on the dispersion properties of CB and $LiCoO_2$ inks in the PVDF and NMP systems. High resolution transmission electron microscopy (HRTEM, JEOL-3010, Japan) was conducted to observe the morphology of the CB. TEM samples were prepared with a highly diluted CB solution (∼0.001 wt%) with the addition of a small amount of surfactant (1 wt% of poly acrylic acid based on CB amount in an aqueous medium). The surface pressure of the CB was calculated from interfacial tension measurements (PAT 2P-USB, Sinterface Technologies, Germany). Scanning electron microscopy (SEM, JSM 5900LV, Jeol, Tokyo, Japan) was performed to observe the microstructural changes in the $LiCoO_2$ electrode when as-received and surface-modified CB were used. The surface roughness was measured using confocal laser microscopy (OLS4000, Olympus, Japan). Confocal microscopes are optical microscopes that display the in-focus region and out-of-focus region as bright and dark, respectively. Furthermore, through the construction of an image that is obtained from the optical sections of specimen taken during the examination, confocal microscopy creates topographic maps. The topographic map is a digital image in which each pixel is assigned a value that represents the z-level. Each pixel may be regarded as an x–y–z coordinate on the three-dimensional surface, which makes it possible to calculate the surface roughness. The detailed information on surface roughness measurement using confocal laser microscopy is detailed elsewhere [22]. The Barrett–Joyner–Halenda (BJH) pore size distribution was measured using BET porosimetry (Autosorb-1, Quantachrome, Boynton Beach, FL, USA) from the desorption branch of the isotherm. It is reported that the method of using the desorption branch of the isotherm is usually more appropriate because the desorption

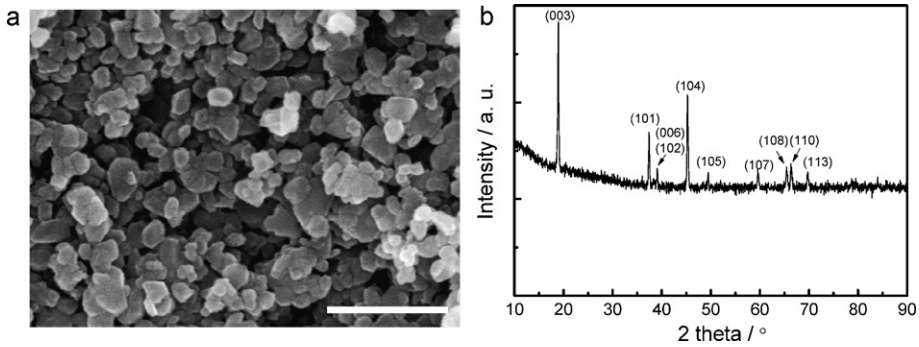

Fig. 1. (a) SEM image and (b) X-ray diffraction patterns of as-synthesized $LiCoO_2$ nanoparticles. The scale bar is 1 μm.

process shows more distinct meniscus control and, thus, is considered to be closer to the true thermodynamic equilibrium than the adsorption branch [23]. To obtain reliable experimental data with an error range of 5%, more than 1 g of electrodes consisting of Al substrate and coating materials ($LiCoO_2$, CB and PVDF) were used for the distribution measurement of the BJH pore size. The net amount of the coating materials ($LiCoO_2$, CB and PVDF) was about 500 ± 30 mg. Coin-type half cells (2016R type) were fabricated in a dry room to evaluate the electrochemical properties of the $LiCoO_2$ electrodes printed with modified and unmodified carbon black. Pure lithium metal foil (Cyprus-Foote Mineral Co., Kings Mountain, NC, USA) was employed as an anode. The electrolyte was 1.3 M $LiPF_6$ in a 3:7 volume mixture of ethylene carbonate (EC) and diethyl carbonate (DEC). To minimize the effect of electrolyte impregnation in the electrode on the electrochemical performance, the assembled coin cells were aged for 24 h at room temperature before electrochemical testing. The coin-type half cells were cycled at a rate of 0.1 C (1 C = 150 mA g^{-1}) for the first cycle, followed by 0.5 C between 3.0 and 4.3 V at 25 °C, using a battery cycle tester (TOSCAT 3000, Toyo systems, Tokyo, Japan). To investigate the effect of the microstructural difference of the electrodes on the electrochemical performance, area-specific impedance (ASI) measurements were performed, which is an effective method to quantitatively determine the overall cell impedance as a function of the depth of discharge (DOD) using the dc interruption technique. ASI measurements were performed on the fifth cycle using a 30-s current interruption method during discharge at the rate of 0.5 C, the details of which can be found elsewhere [24–26].

3. Results and discussion

The SEM image and X-ray diffraction patterns of as-synthesized $LiCoO_2$ powders are shown in Fig. 1(a) and (b), respectively. SEM images indicated that the as-synthesized $LiCoO_2$ powders exhibited an average particle size of about 150 nm, as shown in Fig. 1(a). XRD spectra (Fig. 1(b)) showed that the as-synthesized $LiCoO_2$ particles were well crystallized into phase-pure $LiCoO_2$ particles without any development of a minor phase. Furthermore, the spectra showed a large integrated intensity ratio $I(0\,0\,3)/I(1\,0\,4) = 1.37$ and a clear split of the (1 0 8) and (1 1 0) peaks, which are indicative of an order layered structure. The crystal lattice parameters of the as-synthesized $LiCoO_2$ were $a = 2.819$ Å, $c = 14.070$ Å.

The UV/ozone and TETA treatments made the CB surface hydrophilic by creating oxygen-containing and amino functional groups [19]. Fig. 2 shows the FT-IR spectra of the CB. There was no significant number of functional groups detected on the as-received CB. However, after the UV/ozone treatment, the characteristic absorption bands of the functional groups were observed. The absorption bands observed at 1650 and 3000–3600 cm^{-1} correspond to carboxylic C=O stretching vibrations and O–H stretching in terminal carboxyl groups, respectively [27]. Further treatment using TETA caused additional characteristic absorption peaks around 1660 cm^{-1}, which were related to the vibrations of the amine moiety [28]. The formation of these new functional groups in the CB indicates that its surface became more hydrophilic. There was no morphological change on primary CB particles (Fig. 3), and the CB had almost the same BET specific surface area of about 82 $m^2\,g^{-1}$ regardless of the surface modifications.

The effects of the surface functional groups on the dispersion properties of CB were investigated with a particle size distribution analysis of the CB in PVDF and NMP. As shown in Fig. 4(a), the surface-modified CB in NMP had a significantly smaller particle size than did the as-received CB, with D_{50} values corresponding to 220 nm, 91 nm, and 79 nm for the as-received CB, UV/ozone CB, and UV/ozone–TETA treated CB, respectively. Particle size and distribution are affected by the dispersion properties of solid phases in ink. Poor dispersion results in agglomeration, which makes the particle size distributions of the inks shift to the right, *i.e.*, toward larger particle diameters. Therefore, these results are attributed to the different dispersion properties of the CB in the NMP caused by surface modification. The detailed mechanism to improve the dispersion properties of CB in NMP will be explained in the section evaluating the surface pressure of CB in NMP before and after surface modification.

As mentioned above, the as-received CB has a hydrophobic surface nature and a relatively high Hamaker constant of 6.7×10^{-20} J [14], while NMP has a relatively high polar energy of 12.3 $MPa^{1/2}$ [15]. Therefore, hydrophobic CB agglomerates to some extent in NMP due to this incompatibility. As expected, a surface modification of CB from a hydrophobic to a hydrophilic nature enhanced their compatibility. To confirm the improved

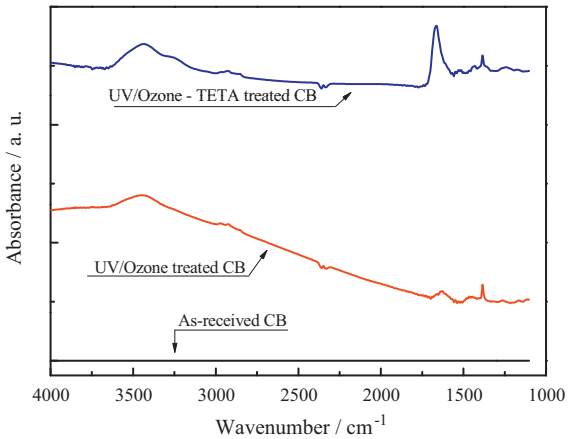

Fig. 2. IR spectra of CB before and after surface modification.

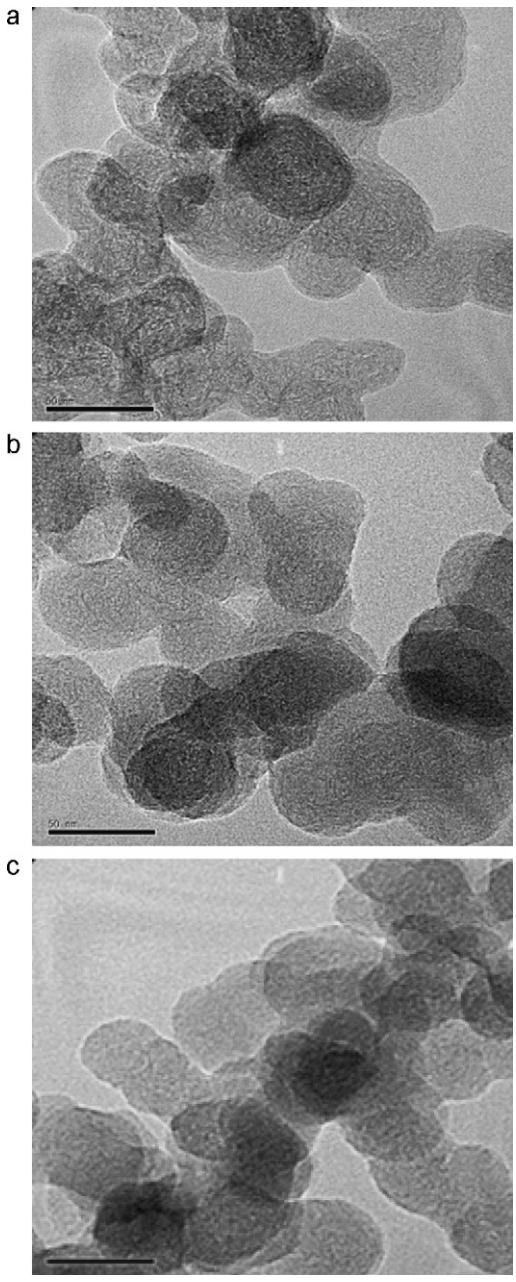

Fig. 3. TEM images of CB after surface modification: (a) as-received CB, (b) UV/ozone-treated CB, (c) UV/ozone–TETA-treated CB. The scale bars are 50 nm.

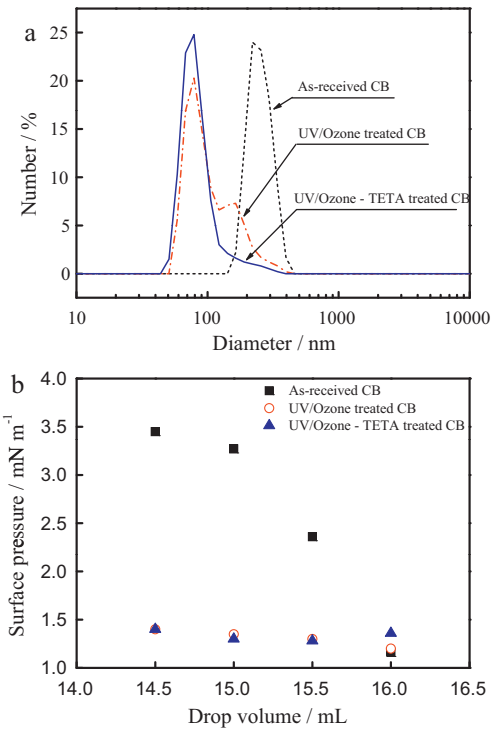

Fig. 4. (a) Particle size distribution, (b) surface pressures of CBs before and after surface modification.

compatibility between surface-modified CB and NMP, the surface pressure of a solution composed of CB and NMP was evaluated by measuring the interfacial tension of the solution. As shown in Fig. 4(b), the surface pressure of the as-received CB in NMP increased with a decrease in drop volume, which could be attributed to the poor compatibility between the CB and NMP causing the CB particles to move toward the air/NMP interface as the drop volume decreased, thereby increasing the surface pressure. On the contrary, surface-modified CB showed a nearly constant surface pressure as the drop volume decreased due to the enhanced compatibility between the CB and the NMP.

Homogeneously dispersed CB would improve the dispersion properties of $LiCoO_2$ ink. In Fig. 5(a), the particle size distributions of the inks prepared with surface-modified CB are shifted to the left, *i.e.*, toward smaller particle diameters, compared to that of the as-received CB. Fig. 5(b) compares the SEM images of electrodes prepared with the as-received CB to those prepared with the surface-modified CB. The electrodes prepared with the surface-modified CB show denser and more homogeneous microstructures than do those prepared with the as-received CB (see the inset of Fig. 5(b)). In addition, the surface-modified CB was more homogeneously distributed around the $LiCoO_2$ particles than the as-received CB, which suggests an improved electrical contact between the surface-modified CB and the $LiCoO_2$. These microstructural differences can be explained through a comparison of the Barrett–Joyner–Halenda (BJH) pore size distributions (Fig. 5(c)) and surface roughnesses (Fig. 6) of electrodes ink-jet-printed with different CB types. The surface modification significantly reduces the large-size pores above 40 nm, which is more prominent for the electrode with UV/ozone–TETA treated CB. The reduced large-size pores result in the reduction of the average pore diameter for the electrode with surface-modified CB. That is, the electrode using surface-modified CB had a smaller pore size distribution compared with electrodes using the as-received CB. The latter electrodes had pores with an average diameter of 45 nm, which is at least 40% as large as those using the surface-modified CB, which had average diameters of 32 nm and 25 nm for the UV/ozone and UV/ozone–TETA-treated CBs, respectively. The electrodes using the surface-modified CB showed a lower surface roughness than those using the as-received CB (Fig. 6). The root mean square (RMS) value reflecting the surface roughnesses of the electrodes using the as-received CB was 0.44 μm, which is larger than that of those using the surface-modified CB, which had RMS values of 0.27 μm and 0.23 μm for the UV/ozone and UV/ozone–TETA-treated CBs, respectively. These microstructural differences can be attributed mainly to differences in the dispersion properties of the $LiCoO_2$ ink. According to Jean, the dispersion properties of particles in the suspension are the main factors in determining the consolidation behavior of packing materials [11]. Furthermore, it is reported that surface roughness is affected by the dispersion properties of solid phase in the ink [29]. Better dispersion properties mean a lower degree of agglomeration in the ink,

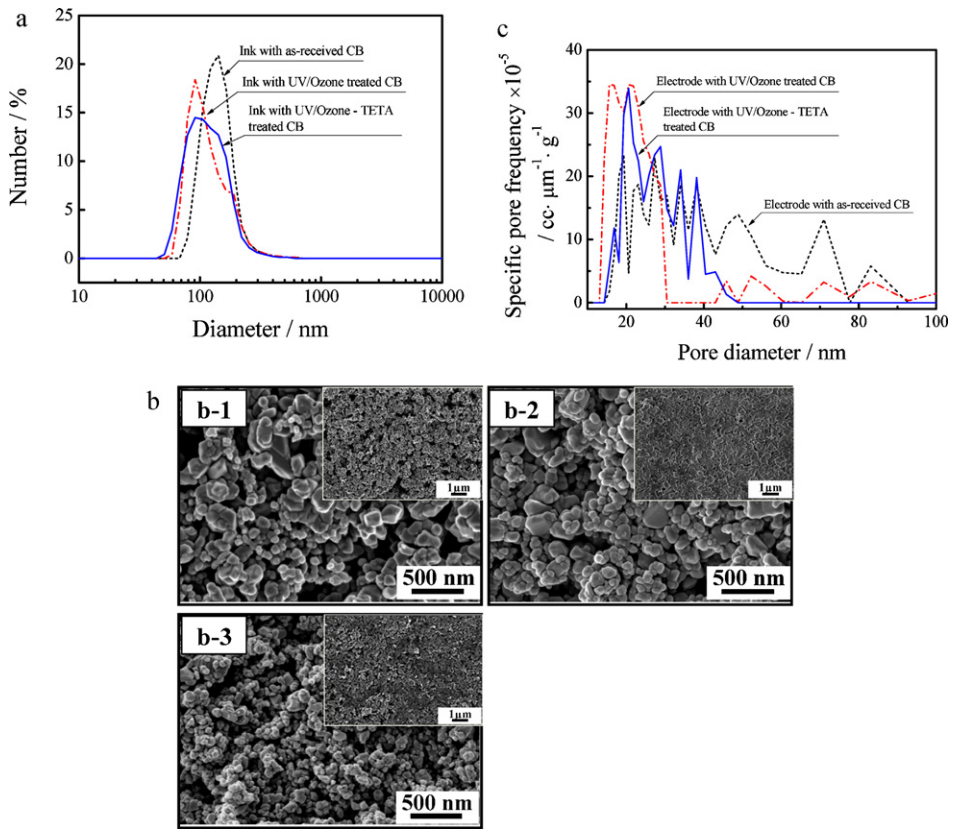

Fig. 5. (a) Particle size distribution of $LiCoO_2$ ink prepared with CBs before and after surface modification, (b) scanning electron microscope images, (c) Barrett–Joyner–Halenda (BJH) pore size distributions of the electrodes prepared with CBs before and after surface modification ($LiCoO_2$:CB:PVDF = 93:3:4).

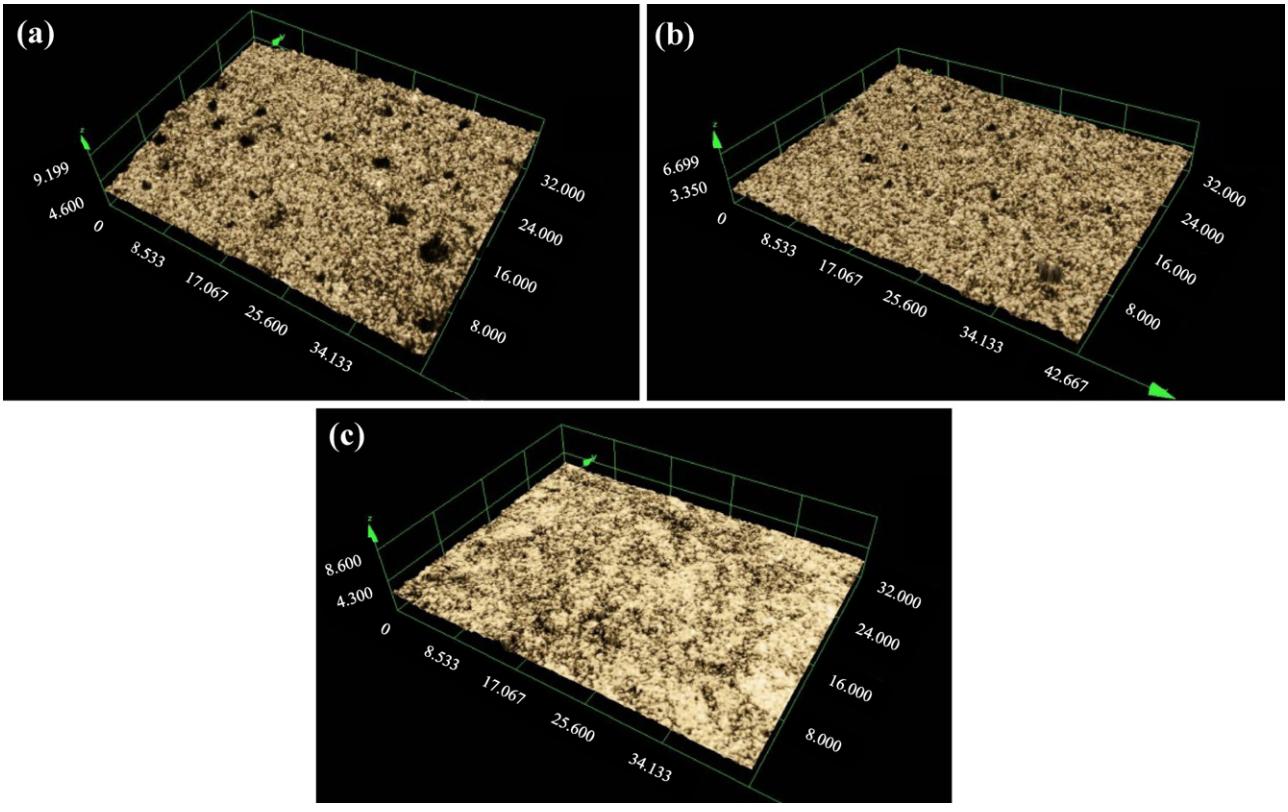

Fig. 6. Confocal scanning microscope images for electrodes prepared with (a) as-received CB, (b) UV/ozone-treated CB, (c) UV/ozone–TETA-treated CB ($LiCoO_2$:CB:PVDF = 93:3:4). The units are microns.

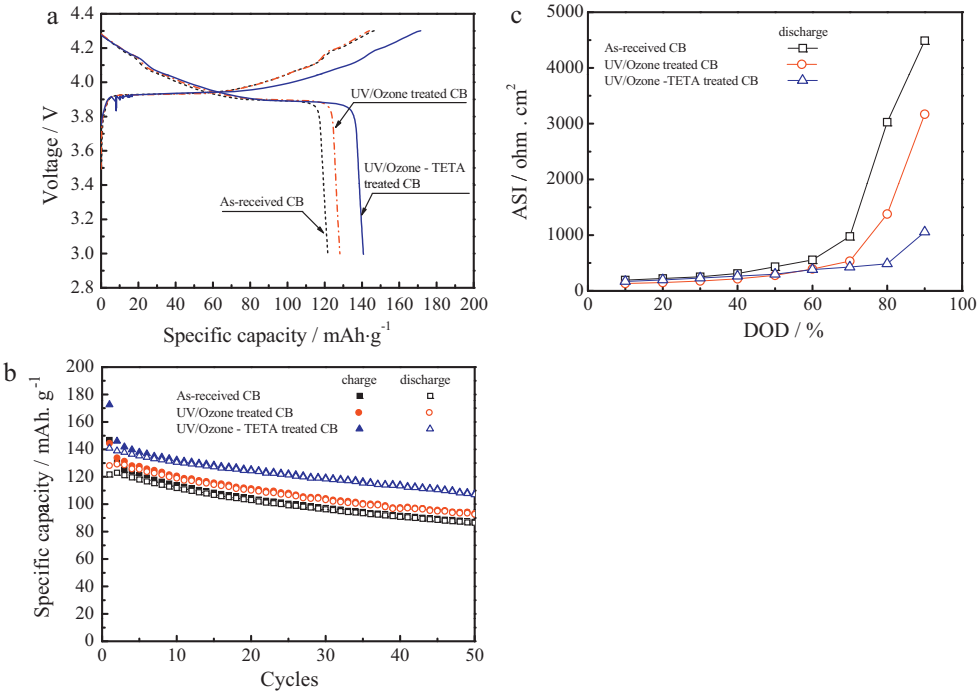

Fig. 7. (a) Initial voltage profiles, (b) charge–discharge curves as a function of cycle number: cycled at a rate of 0.1 C (1 C = 150 mA g^{-1}) for the first cycle, followed by 0.5 C between 3.0 and 4.3 V at 25 °C using a battery cycle tester, (c) ASI on the fifth cycle as a function of DOD for an ink-jet-printed $LiCoO_2$ electrode with CBs before and after surface modification ($LiCoO_2$:CB:PVDF = 93:3:4).

which leads to a lower surface roughness and more homogeneous microstructures [29]. Therefore, improvement of the dispersion properties of CB due to surface modification leads to homogeneous distribution around each $LiCoO_2$ particle, creating a dense, uniform microstructure.

Fig. 7 shows the electrochemical properties of ink-jet-printed $LiCoO_2$ electrodes. The initial discharge capacities for the electrodes using surface-modified CB were higher than the one using as-received CB. In particular, the electrode using UV/ozone–TETA-treated CB had the highest initial discharge capacity among the electrodes investigated. The discharge capacities for the electrodes using as-received, UV/ozone, and UV/ozone–TETA-treated CB were 121.6, 128.2, and 140.8 mAh g^{-1}, respectively, a trend that is consistent with that of the dispersion properties, which is a function of the surface functional group. The improved specific discharge capacities of electrodes using surface-modified CB can be attributed to the modified microstructure of the electrode in which the CB was more homogeneously dispersed, improving the electrical contact between the CB and $LiCoO_2$ nanoparticles. It can be understood through a comparison of the ASI of the electrode as a function of DOD. As shown in Fig. 7(c), the electrodes using surface-modified CB exhibited considerably lowered ASI values compared to those using the as-received CB, suggesting that surface modification of the CB could improve the electrical conductivities of electrodes.

4. Conclusions

UV/ozone and triethylenetetramine (TETA) were exploited for the surface functionalization of carbon black to improve its dispersion properties in ink used for printed $LiCoO_2$ thin film electrodes. UV/ozone and TETA treatments caused the carbon black surface to become more hydrophilic and improved the dispersion properties of the carbon black and $LiCoO_2$ ink. The electrodes prepared with surface-modified carbon black had denser and more homogeneous microstructures compared to the electrodes using as-received carbon black. The electrochemical performance indicated that the electrodes with surface-modified carbon black exhibited improved discharge capacities, which were caused by better electrical contact between the carbon black and the $LiCoO_2$.

Acknowledgements

This work was financially supported by the National Research Foundation of Korea (NRF) through a grant (K2070400000307A050000310, Global Research Laboratory (GRL) Program) provided by the Korean Ministry of Education, Science & Technology (MEST) in 2009, by the IT R&D program of MKE/KEIT [10035379, Rollable secondary battery for mobile IT device], and by the Samsung Advanced Institute of Technology, Samsung Electronics Co. Ltd.

References

[1] H. Nishide, K. Oyaizu, Science 319 (2008) 737–738.
[2] Y.J. Park, K.S. Park, J.G. Kim, M.K. Kim, H.G. Kim, H.T. Chung, J. Power Sources 88 (2000) 250–254.
[3] S.C. Nam, Y.S. Yoon, W.I. Cho, B.W. Cho, H.S. Chun, K.S. Yun, Electrochem. Commun. 3 (2001) 6–10.
[4] K.H. Kim, S.I. Pyun, K.N. Jung, Electrochim. Acta 52 (2006) 152–160.
[5] S.C. Nam, C.H. Paik, W.I. Cho, B.W. Cho, H.S. Chun, K.S. Yun, J. Power Sources 84 (1999) 24–31.
[6] R.Z. Hu, M.Q. Zeng, M. Zhu, Electrochim. Acta 54 (2009) 2843–2850.
[7] Y. Zhao, Q. Zhou, L. Liu, J. Xu, M. Yan, Z. Jiang, Electrochim. Acta 51 (2006) 2639–2645.
[8] J. Huang, J. Yang, W. Li, W. Cai, Z. Jiang, Thin Solid Films 516 (2008) 3314–3319.
[9] K. Dokko, J. Sugaya, H. Munakata, K. Kanamura, Electrochim. Acta 51 (2005) 966–971.
[10] M.S. Kwon, J. Choi, H. Kim, S. Doo, 214th ECS Meeting, 2008 (Abstract # 680).
[11] J.H. Jean, Mater. Chem. Phys. 40 (1995) 285–290.
[12] T.J. Patey, A. Hintennach, F. La Mantia, P. Novak, J. Power Sources 189 (2009) 590–593.
[13] R. Dominko, M. Gaberscek, J. Drofenik, M. Bele, J. Jamnik, Electrochim. Acta 48 (2003) 3709–3716.
[14] K.C. Ruthiya, J. van der Schaaf, B.F.M. Kuster, J.C. Schouten, Chem. Eng. Sci. 60 (2005) 6492–6503.
[15] C.M. Hansen, Hansen Solubility Parameters: A User's Handbook, CRC Press, 2000.

[16] F.H. Gojny, J. Nastalczyk, Z. Roslaniec, K. Schulte, Chem. Phys. Lett. 370 (2003) 820–824.
[17] R. Yu, L. Chen, Q. Liu, J. Lin, K.L. Tan, S.C. Ng, Chem. Mater. 10 (1998) 718–722.
[18] P. Poncharal, C. Berger, Y. Yi, L. Wang, W.A. de Heer, J. Phys. Chem. B 106 (2002) 12104–12118.
[19] M.L. Sham, J.K. Kim, Carbon 44 (2006) 768–777.
[20] A. Wijayasinghe, B. Bergman, C. Lagergren, Electrochim. Acta 49 (2004) 4709–4717.
[21] H. Xia, H. Wang, W. Xiao, L. Lu, M.O. Lai, J. Alloys Compd. 480 (2009) 696–701.
[22] D.A. Lange, H.M. Jennings, S.P. Shah, J. Mater. Sci. 28 (1993) 3879–3884.
[23] IUPAC Recommendations, Pure Appl. Chem. 66 (1994) 1739.
[24] T.D. Kaun, P.A. Nelson, L. Redey, D.R. Vissers, G.L. Henriksen, Electrochim. Acta 38 (1993) 1269–1287.
[25] I. Belharouak, C. Johnson, K. Amine, Electrochem. Commun. 7 (2005) 983–988.
[26] J.S. Hong, H. Maleki, S.A. Hallaj, L. Redey, J.R. Selman, J. Electrochem. Soc. 145 (1998) 1489–1501.
[27] J. Zhu, H. Peng, F. Rodriguez-Macias, J.L. Margrave, V.N. Khabashesku, A.M. Imam, K. Lozano, E.V. Barrera, Adv. Funct. Mater. 14 (2004) 643–648.
[28] J. Zhu, J.D. Kim, H. Peng, J.L. Margrave, V.N. Khabashesku, E.V. Barrera, Nano Lett. 3 (2003) 1107–1113.
[29] E.S. Thiele, N. Setter, J. Am. Ceram. Soc. 83 (2000) 1407–1412.